

Research Paper

Unsteady forced convection over cylinder with radial fins in cross flow



Sajjad Bouzari, Jafar Ghazanfarian*

Faculty of Engineering, Department of Mechanical Engineering, University of Zanjan, University Blvd., 45371-38791 Zanjan, Iran

HIGHLIGHTS

- The unsteady flow over finned cylinder is investigated.
- The effect of sharp edges on the St and secondary frequencies was discussed.
- The highest Nu relative to the drag coefficient was obtained for 2 fins.
- The highest effectiveness was obtained for the case with 4 fins.
- By increasing Re the highest effectiveness increases.

ARTICLE INFO

Article history:

Received 1 July 2016

Revised 22 September 2016

Accepted 9 October 2016

Available online 11 October 2016

Keywords:

Heat transfer augmentation

Forced convection

OpenFOAM

Strouhal number

Fin effectiveness

ABSTRACT

The effect of adding straight fins on thermal and hydraulic characteristics of transient heat and fluid flow over a circular cylinder is investigated using the OpenFOAM toolbox. Simulations are conducted at Reynolds numbers of 100, 112.5, 125, 137.5, 150, 200, and the dimensionless fin height of 0.15, 0.35, 0.75, 1.5. It is found that in spite of flow over naked circular cylinder, which has one dominant vortex shedding frequency, in the case of finned cylinder some minor frequencies appear. The appearance of secondary peaks which originates from the existence of sharp edges in the geometry makes it possible to capture the lock-on phenomenon in several frequencies. It is computed that the mean drag coefficient increases as the fins are lengthened, and decreases as the number of fins is enhanced. Also, it is found that the average Nusselt number faces a decrease with the increase the number of fins. Finally, the best Nu/C_d ratio was obtained for the case with 2 parallel-flow horizontal fins. Also, the fin effectiveness has been calculated for cylinder with different number and heights of fins in various Reynolds numbers, and it is concluded that the best number of fins with the highest effectiveness for all Reynolds numbers is equal to 4.

© 2016 Elsevier Ltd. All rights reserved.

1. Introduction

The concept of flow over bluff bodies is imperative due to the understanding of the mechanism of von-Karman vortex street to control the flow and boundary layer behavior. Such studies bring a great opportunity to figure out the underlying physics of similar problems, and to generate some data that can be used for the validation of simulations conducted for more complex geometries. Despite the fact that the understanding of flow past bluff bodies has been a subject of interest to engineers for decades, but because of the formation of complex wakes, and the interaction of three shear-layers, namely the boundary layer, the separated free shear-layer, and the wake; there are lots of questions remained unsolved.

The idea of adding fins for the purpose of augmenting heat transfer is a common way in many industrial applications. The addition of fins dramatically changes the flow regime, which usually results in the simultaneous increase of the heat transfer rate and the drag force. The vortex shedding frequency (or the Strouhal number in its dimensionless form) is one of the most important parameters in such problems, because of the occurrence of the lock-on phenomenon, which originates from the synchronization of two dominant frequencies. The importance of the transient flow simulation over such complex geometries lies on the fact that the addition of sharp edge fins noticeably changes the flow regime and vortex shedding frequency.

A collection of studies about flow over cylinder can be divided into four different categories. The first category is devoted to the flows over stationary cylinder. The history of this field goes back to almost 100 years. In one of the first studies Roshko [1] held a study on drag coefficient and vortex shedding frequency. Gerrard

* Corresponding author.

E-mail address: j.ghazanfarian@znu.ac.ir (J. Ghazanfarian).

Nomenclature

C_d	drag coefficient $\left(\frac{F_d}{1/2\rho U_\infty^2 D^2}\right)$	<i>Greek</i>	
C_l	lift coefficient $\left(\frac{F_l}{1/2\rho U_\infty^2 D^2}\right)$	α	thermal diffusivity ($\text{m}^2 \text{s}^{-1}$)
D	diameter (m)	ν	kinematic viscosity ($\text{m}^2 \text{s}^{-1}$)
F_d	drag force (N)	ρ	density (kg m^{-3})
F_l	lift force (N)	ξ	fin effectiveness
h	fin length (m)	<i>superscript</i>	
H	dimensionless fin length $\left(\frac{h}{D}\right)$	*	normalized condition
k	conductivity ($\text{W m}^{-1} \text{K}^{-1}$)	<i>subscript</i>	
Nu	Nusselt number $\left(\frac{hD}{k}\right)$	i	component
p	pressure (Pa)	s	surface
PD	power density	avr	average value
Pr	Prandtl number $\left(\frac{\nu}{\alpha}\right)$	∞	upstream
Re	Reynolds number $\left(\frac{U_\infty D}{\nu}\right)$	0	initial condition
St	Strouhal number $\left(\frac{fD}{U_\infty}\right)$		
t	time (s), tangential coordinate (m)		
T	temperature (K), perimeter (m)		
U	velocity (m s^{-1})		
x	coordinate (m)		

[2] discussed about the vortex formation mechanisms and various patterns, and Eckert [3] studied the heat transfer from circular stationary cylinder. Cseryei and Straatman [4] presented the convective heat transfer on horizontal cylinder due to a bank of vertically oriented circular jets. Seyf et al. [5] presented the flow and thermal investigation of nanoencapsulated phase-change-material slurry past an unconfined square cylinder. A complete review on this class of studies can be found in Williamson [6].

The second category consists of papers scrutinizing the flow over oscillating cylinders. Koopman [7] presented the influence of forced transverse oscillation of cylinder on the vortex shedding frequency, and reported the occurrence of lock-on condition. Nobari and Ghazanfarian [8] performed a research on flow over rotating cylinder with cross flow oscillation, and compared the drag and lift coefficients with the results of stationary cylinder. In another study, Ghazanfarian and Nobari [9] studied the heat transfer enhancement by the oscillating of a rotating cylinder.

The third category is about the effect of added drag-reductive shields such as splitters on the flow over cylinder. Assi and Bearman [10] conducted experiments on the galloping response of a circular cylinder fitted with three different splitter plates free to oscillate transverse to a stream and considered variations in plate length and plate porosity. Qiu et al. [11] studied the aerodynamic differences between the bare cylinder and cylinders with frontal, wake and bilateral splitter plates. They found that a frontal splitter plate, with plate length to cylinder diameter ratio of $L/D = 3$ has produced a postcritical flow at relatively low Reynolds numbers by the generated disturbances in the approaching flow. Hwang and Yang [12] studied the drag reduction on a circular cylinder using dual detached splitter plates with the same length as the cylinder diameter (d), which one splitter is placed along the horizontal centerline and the other is in the near-wake region. They reported that the drag force varies with both gap ratios with a minimum value at a certain set of gap ratios for each Reynolds number. In other study, Bayram et al. [13] implemented the effect of upstream splitter on the flow pattern.

The fourth category of studies is dedicated to the flow over finned cylinder. Haldar et al. [14] carried out a conjugate numerical solution of laminar free convection about a horizontal cylinder with external longitudinal fins of finite thickness. Sajedi et al. [15] numerically and experimentally studied the external extended finned tube heat exchanger, they have conducted set of experi-

ments in different Reynolds and Reyleigh numbers in order to obtain the optimized fin numbers. Abuhijleh [16] accomplished the simulation of flow over cylinder with radial fins in steady state flow regime at low Reynolds numbers. This paper just discusses about the thermal field by illustrating the variation of Nusselt number, and ignores the influence of fin's geometry on the flow pattern.

The 3D numerical simulations of nanofluid flow over micro-pin-fin heat sinks with circular [17] and elliptical [18] cross sections were implemented with applications in phase-change-materials [19]. The application of extended surfaces for arrays of tubes was investigated for staggered circular pin finned tube banks [20], H-type finned tube bank in a fully developed region [21], small helically segmented finned tube bank [22], and solid circular finned tube bundles [23]. Also, there are many papers devoted to the various applications of heat transfer analysis for enhancement purposes in thermo-photovoltaics [24], nanoscale actuators [25], entropy generation in nanofluid flows [26], phase-change-material [27], cellulosic evaporative cooling pads [28], the resin transfer molding process [29], the vapor flow analysis [30], and the nanofluid pulsating heat pipe [31].

In this study we are to fill the gap exists in the transient simulation of both flow and temperature fields over finned cylinder. Fins are radially attached to the cylinder, and assumed to have high thermal conductivity. Examination of such kind of fin orientation is less considered in literature by taking into account passable details. In Section 2, the governing equations including the full Navier-Stokes' equations, the energy equation, and the continuity equation are introduced. In Section 3, the governing equations have been discretized by finite volume method on the platform of OpenFOAM codes with the solver of ThermalPimpleFOAM. After verifying the numerical results in Sections 4 and 5 presents the results of simulations conducted at moderate Reynolds numbers in the range of 100–200 considering different number of fins and various heights. The major vortex shedding frequencies with and without fins are calculated, and the effects of fins on the variation of Strouhal number, the drag coefficient, and the Nusselt number have been investigated among results.

2. Governing equations

The governing equations of two-dimensional incompressible viscous flow of Newtonian fluid over a cylinder with fins are con-

sidered in this section. The balance of mass, momentum, and energy can be written in their non-dimensional form as

$$\frac{\partial U_i^*}{\partial x_i^*} = 0, \quad (1)$$

$$\frac{\partial U_i^*}{\partial t^*} + U_i^* \frac{\partial U_i^*}{\partial x_i^*} = -\frac{\partial p^*}{\partial x_i^*} + \frac{1}{Re} \frac{\partial^2 U_i^*}{\partial x_j^* \partial x_j^*}, \quad (2)$$

$$\frac{\partial T^*}{\partial t^*} + U_i^* \frac{\partial T^*}{\partial x_i^*} = \frac{1}{RePr} \frac{\partial^2 T^*}{\partial x_j^* \partial x_j^*}, \quad (3)$$

where U_i^* denotes the non-dimensional velocity component with respect to the inlet velocity. T^* is the non-dimensional temperature, p^* is the non-dimensional pressure normalized with the dynamic pressure, Pr is the Prandtl number, and Re is the Reynolds number defined based on the cylinder's base diameter. The definitions of the governing dimensionless parameters are as follows.

$$x^* = \frac{x}{D}, \quad t^* = \frac{tU_\infty}{D}, \quad U^* = \frac{U}{U_\infty}, \quad H = \frac{h}{D}, \quad p^* = \frac{p}{\frac{1}{2}\rho U_\infty^2},$$

$$T^* = \frac{T - T_\infty}{T_s - T_\infty}, \quad (4)$$

$$Re = \frac{U_\infty D}{\nu}, \quad Pr = \frac{\nu}{\alpha}, \quad (5)$$

where H is the dimensionless form of the fin height. Other post-processing dimensionless groups are defined as

$$C_l = \frac{F_l}{\frac{1}{2}\rho U_\infty^2 D^2}, \quad C_d = \frac{F_d}{\frac{1}{2}\rho U_\infty^2 D^2}, \quad St = \frac{fD}{U_\infty}, \quad \zeta = \frac{Q_{fin}}{Q_{nofin}},$$

$$Nu = \frac{hD}{k}, \quad (6)$$

where f , Q , ζ are the frequency of vortex shedding, the heat transfer rate, and the fin effectiveness, respectively. The definitions of other parameters are presented in the nomenclature. The value of average Nusselt number is computed based on

$$Nu_{avr} = \frac{1}{T} \int_T Nu(t) dt, \quad (7)$$

where T is the perimeter of the cylinder including fins, dt is the differential element of the surface, t is the surface tangential coordinate, and $Nu(t)$ is the local Nusselt number. Due to the transient nature of the vortex shedding, the value of Nu_{avr} varies with time. So, a similar averaging process should be performed to calculate the spatio-temporal mean magnitude of the Nusselt number.

In this paper, the Fourier's law and the Newton's viscosity law were considered as constitutive relations. The body force, the energy source term, and the friction heat dissipation were neglected. The main non-dimensional parameters are the Reynolds number, the Prandtl number, and fin's height H , which is non-dimensionalized with respect to the cylinder radius.

The accuracy of laminar flow assumption has been validated by the experimental data [32], and was successfully used by other researchers [33–35]. Jiin-Yuh and Jyh-Yan [32] presented the flow over a four-row tube bank with the elliptic and circular finned tubes at $20,000 < Re < 80,000$. They did experiments and compared the numerical laminar results with the experimental data in such high Re numbers. Lemouedda et al. [33] developed a comparative study on heat transfer for different fin geometries. Simulations were carried out for the laminar air flow at Reynolds number of 600–2600. They declared that for external flows across cylindrical tubes, the boundary layer on the cylinder remains laminar for $Re < 200,000$, and the transition may occur in the free shear-layers behind the cylinder. The drag reduction on a circular cylinder using dual

detached splitter plates was numerically studied at $Re = 100, 160$ [34]. Laminar flow over a circular cylinder with detached short splitter-plates was numerically simulated in order to assess the suppression of periodic vortex shedding at $Re = 100, 150$ [35].

In addition, the assumption of laminar flow was also done in papers involving the flow over oscillating cylinders [36,8]. The only trace of transition to turbulent was inspected near the upper bound of the lock-on region when the frequency of oscillation is higher than 1.3 times the Strouhal frequency. This case was discussed by Karniakadis and Triantafyllou in detail [36], and was announced by [8]. They declared that due to the presence of chaos, the peak of FFT diagram has been widened. A similar phenomenon of turbulence appearance once the local Reynolds number is lower than the critical Reynolds number was presented in an internal flow case by Ghazanfarian and Ghanbari [37].

Since the Reynolds number is very far from the critical transition Reynolds number for similar geometries such as cylinder and sphere, we can be sure about the validity of the laminar flow assumption. In such problems, the first regime is steady flow, then the vortex shedding starts and the flow becomes unsteady 2D, then the three-dimensionality effects appear, and very later the flow becomes turbulent. In this paper we are dealing with the second regime. On the other hand, in order to more closely deal with the local transition to turbulence, an instability analysis should be performed to calculate the local instability condition of flow over such geometries. Since this process is not straightforward, we can use the available instability analysis for similar geometries such as square cylinder with sharp edges [38] to estimate the instable Reynolds number, and conservatively select a lower Re .

3. Geometry and numerical scheme

The open-source field operation and manipulation (OpenFOAM) software written in C++ [39] version 2.3 has been used to solve the governing equations with the finite volume technique. The second-order upwind scheme was used to deal with the convective terms, and the second-order Gauss-linear approach to handle the diffusion terms. There are some other studies involving high gradients in flows such as supersonic flows [40,41], the LES modeling [42], unsteady flows [43], fuel cells [44] and have used the Gauss linear scheme. In addition, the fourth-order least-squares scheme was also tested to discretize the gradient terms, and it is obtained for the Nusselt number computation that the relative error of using the second-order scheme is about 0.2%. In this study, higher gradients appear normal to the surface of cylinder and along the fin tips. An effective way to handle such gradients is to use finer meshes in such regions. So, the boundary layer mesh with sufficient number of elements along tips were used to be sure about correctly capturing the high gradients in these critical areas.

The Euler method is used for the local time derivative, and the gradient term is reconstructed by the Gauss linear method. The pressure-implicit with splitting of operators (PISO) algorithm is applied for the pressure-velocity coupling. The under-relaxation factors for all equations are set to 0.7, and the threshold of residuals, which were defined based on the infinity norm for each time-step is equal to 10^{-6} .

The geometry of problem and the required boundary conditions employed in the numerical procedure are shown in Fig. 1. As seen in Fig. 1, the attached fins are placed in a way that the first and the last fins are parallel with the upstream flow direction. In this way, these two fins, respectively, act like upstream and downstream splitters which can control the flow pattern to reduce the exerted drag force. The Prandtl number for all cases is 0.7, and all fins have a normalized thickness of 0.003 with respect to the cylinder's diameter.

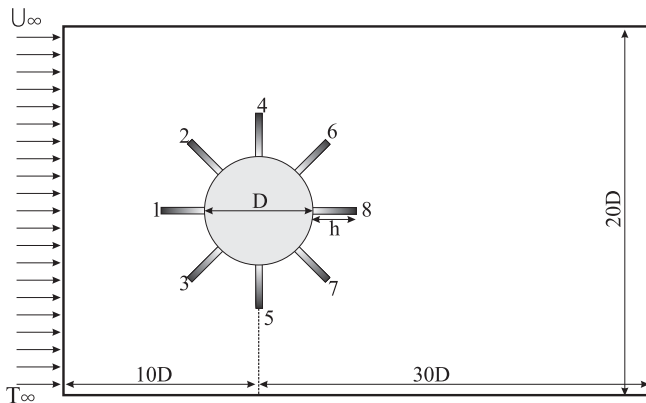


Fig. 1. Schematic geometry of problem, boundary conditions, and the fin numbering style.

A uniform velocity profile enters the domain, and the slip boundary condition is applied over the top and bottom side walls. The cylinder and fins are assumed to be iso-thermal with the magnitude of T_s . The uniform temperature of T_0 is applied for the entrance thermal condition. The zero-gradient boundary condition has been set for the pressure and temperature at the outlet of computational domain. It should be noted that the thermal resistance of fins has been neglected due to the high conductivity of fin's construction material such as Aluminum, and also their very small thickness. So, the temperature gradient within the fins is nearly zero, and the cylinder's surface temperature distributes over the whole perimeter of fins.

In order to check the sensitivity of results to the grid size, the computations have been performed on the cylinder with 8 fins corresponding to four different mesh sizes. The details of the best grid is shown in Fig. 2, and the number of elements of different grids used are given in Table 1. The values of the average Nusselt number at Reynolds number of 10 for flow over cylinder with 8 fins, and the non-dimensional height of 0.35 have been computed using four different grids, and the results obtained are listed in Table 1. It is clear that for the domains with the numerical grid finer than case 3 with 36,789 elements, the average Nusselt number is not sensitive to the grid size. As shown in Fig. 2a in a close snapshot, the boundary layer mesh is used near the surface of cylinder to deal with the high gradients due to the viscous effect. Also, 4 elements are required on the tip of fins to correctly capture the streamwise sharp local gradients of temperature normal to the surface.

The numerical predictions are also analyzed with respect to the different time-step sizes. To do so, simulations were conducted for four different time-step sizes for the case of a cylinder with 8 fins, and the non-dimensional height of 0.35. This analysis resulted in the best time-step-size of 0.005 s.

4. Numerical code accuracy

The accuracy of the numerical code is tested by evaluating the obtained numerical results with the available experimental data. The first case deals with the variation of the Strouhal number with respect to the Reynolds number for the cylinder without fins. As shown in Fig. 3, there is a good agreement between the experimental data of Williamson [6] and the current computational results. It should be noted that the Strouhal number is obtained based on the main frequency of the lift force, which is computed by applying the fast Fourier transform (FFT) to the time history of the lift coefficient.

In order to assess the accurateness of the solver, the drag coefficient have been compared with experimental and numerical

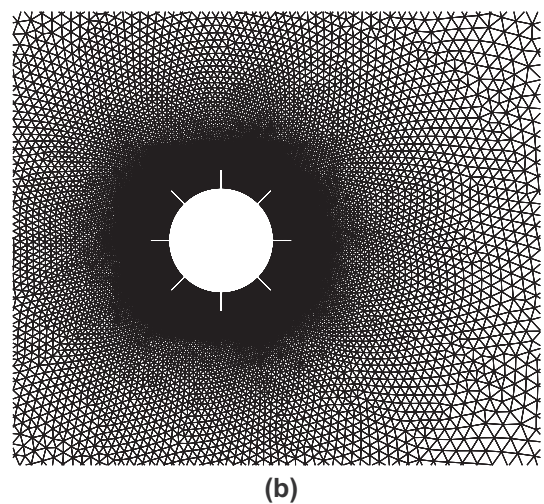
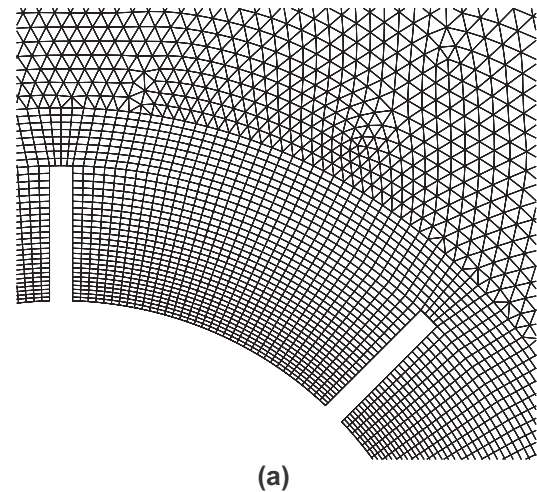


Fig. 2. Structured grid near the cylinder and unstructured grid in the surrounding, (a) grid close up and boundary layer elements in the vicinity of cylinder, (b) the overall view.

Table 1

The grid independence test for flow over cylinder with 8 fins with the non-dimensional height of 0.35 at $Re = 10$.

	Number of elements	Average Nusselt number
1	18,473	1.23
2	23,256	1.31
3	36,789	1.38
4	45,360	1.39

results of Henderson [47] and Park [48] in Table 2. Also, the validation of Nusselt number is done at different Reynolds numbers for the case of unfinned cylinder using the correlations presented by Hilpert [49] and Churchill and Burstain [50] in Table 3.

To check the correctness of the solution of energy equation for finned case, the local Nusselt number of the cylinder with 6 fins of height 0.35 times the cylinder's radius is compared with the numerical results of [16] in Fig. 4. The Reynolds number and the Prandtl number are 20 and 0.7, respectively. Due to the symmetry of the flow field at small Reynolds number, the simulations were conducted and the results were illustrated for a half cylinder. Also, the arrangement of extended surfaces is composed of three fins on the half cylinder similar to what presented by Abuhijleh [16]. As obvious from Fig. 4, in this case the fins attached to the upstream and downstream stagnation points were omitted.

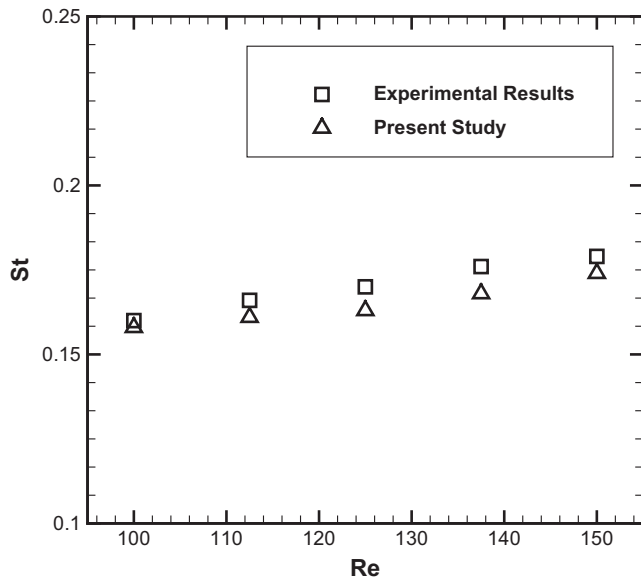


Fig. 3. Comparison of Strouhal number variation with respect to the Reynolds number for cylinder without fins with the empirical results of Williamson [6].

Table 2

Comparison of computed drag coefficients at various Reynolds numbers for an unfinned cylinder.

Re	Present study	Henderson [47]	Park [48]
100	1.42	1.35	1.33
112.5	1.40	1.35	-
125	1.39	1.39	1.32
137.5	1.38	1.36	-
150	1.38	1.35	1.32
200	1.38	1.34	-

Table 3

Validation of average Nusselt number for various Reynolds Numbers for an unfinned cylinder.

Re	Present study	Hilpert [49]	Churchill and Bernstein [50]
100	5.27	5.19	5.16
112.5	5.60	5.50	5.45
125	5.91	5.75	5.73
137.5	6.22	6.02	6.00
150	6.51	6.26	6.26
200	7.50	7.16	7.19

As it is obvious from Fig. 4, there is a good agreement between the variation of local Nusselt number reported by Abuhijleh [16] and those of present study. It should be noted that in order to avoid numerical complexities originating from the non-zero thickness of fins, Abuhijleh [16] ignored the fin thickness, and assumed the fin structure as flat plates coinciding with the computational nodes. This presumption will lead to non-physical capturing of gradients near the top edge of fins, which will lead to the incorrect computation of averages. Consequently, deviations can be seen between the results of our study and those of Abuhijleh [16] near the sharp trailing edges of fins.

5. Results and discussion

After verifying the exactness of the solver, simulations are conducted for the case of flow past a cylinder with 2, 4, 6, 8, and 10 radially attached fins with the non-dimensional height of 0.15, 0.35, 0.75, 1.5 at the Reynolds number of 100, 112.5, 125, 137.5,

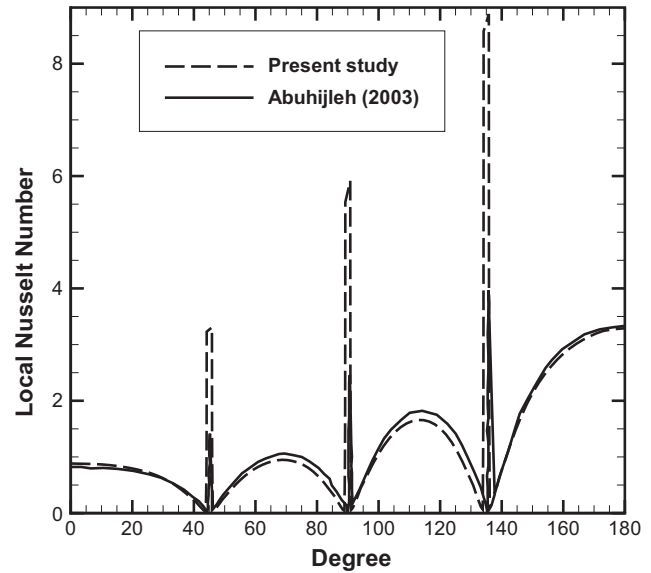


Fig. 4. Comparison of distribution of local Nusselt number along the perimeter with results reported by Abuhijleh at Reynolds number of 20 [16].

150, 200. Results include the frequencies analysis of vortex shedding, the flow and temperature patterns, and the trends of the drag coefficient, the Nusselt number, and the fin effectiveness.

It is worth noting that by increasing the Reynolds number; gradually the three-dimensionality effects appear in the flow field. Although there are papers about the critical Re above which the flow should be muller over as 3D for square [38] and circular [45] cylinders, but no scientific text is available for the determination of a criteria for the three-dimensionality of flow over complex geometries such as finned cylinder. So, In this paper the maximum Re number of 200 has been conservatively chosen.

Fig. 5 illustrates the vorticity and temperature fields for flow over cylinder with 8 fins and non-dimensional height of 0.35 at $Re = 150$ during one period of vortex shedding. Since, the fluid acts like an entirely deforming medium, the power density spectrum of the lift force consists of infinite number of frequencies. However, some major amplitude can be captured, which shows the main dominant frequency of the exerted force. However, the presence of sharp trailing edges of attached fins causes the manifestation of secondary small eddies near the separation points. The main vortex and the secondary vortices shedded near the end of fins number 6 and 7, in three different times during one period of vortex shedding, can be seen in Fig. 5. It is interesting that the secondary vortices have different frequencies from the main vortex, and the number of secondary vortices is totally related to the number of sharp fin tips, which alter the vortex shedding pattern. Also, it is obvious from the vorticity contours that the high pressure zone near the stagnation point is confined to the tip of the first fin. This fact leads to the reduction of the form drag component of the drag force.

Fig. 6 shows the transformation of temporal variation of the lift coefficient into the frequency domain by applying the fast Fourier transformation (FFT) in which the vertical axis is the power density, and the horizontal axis is the spectrum of dimensionless frequencies. Here, the FFT was taken over the dimensionless series of C_l versus dimensionless time. So, the unit of PD is $1^2 \times 1 = 1$. Since, the medium of a fluid which streams over a bluff body makes a continuous deforming material, finding a finite number of frequencies for the exerted force is not logical. Inversely, there should be a continuous range of frequencies in which some frequencies have dominant amplitude.

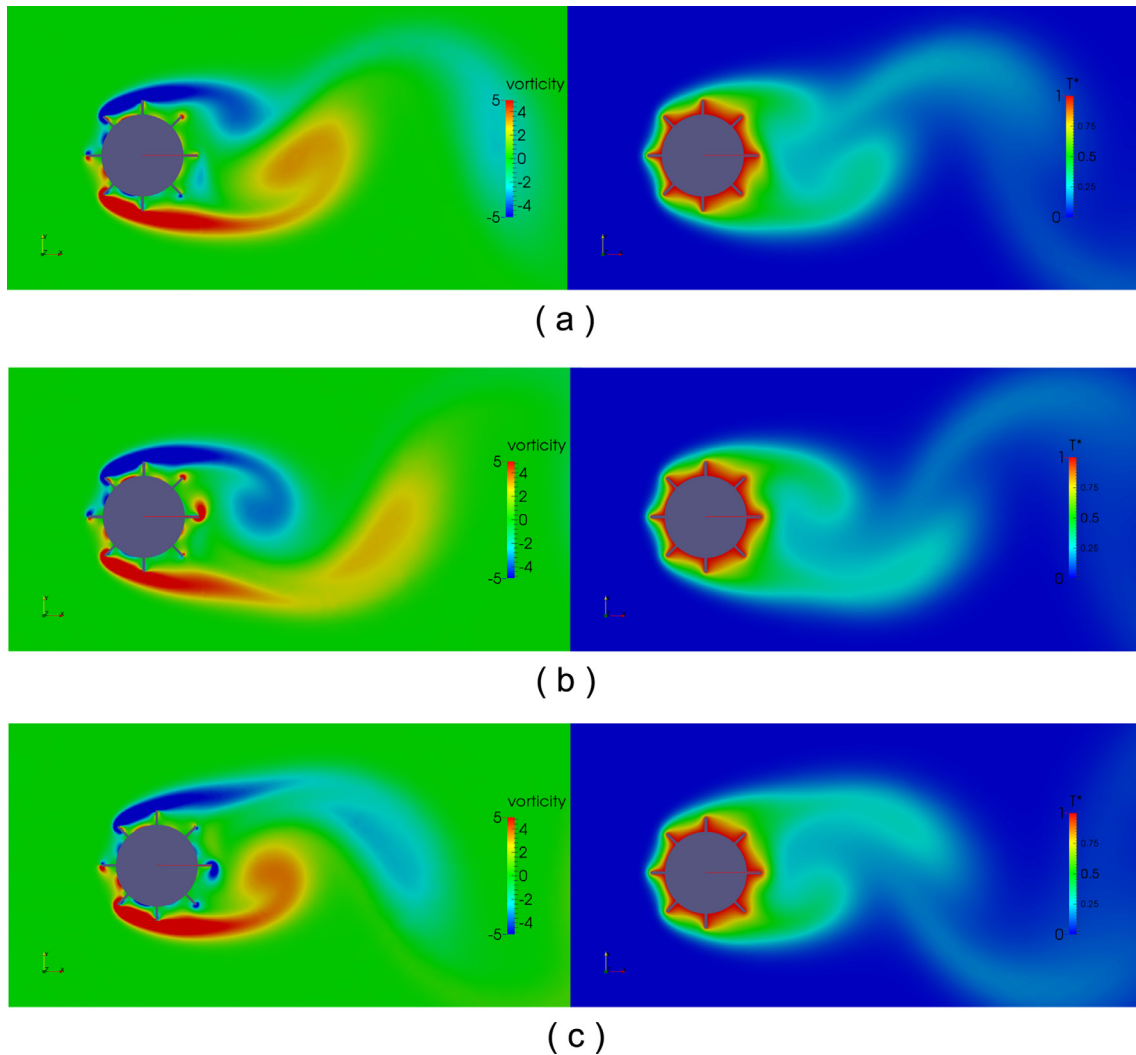


Fig. 5. The vorticity and normalized temperature contours for flow over cylinder with 8 fins with non-dimensional height of 0.35 at Reynolds number of 150 in (a) the beginning, (b) the first quarter, (c) the third quarter of one period of vortex shedding.

The FFT diagram of the lift coefficient induced by the flow over a simple cylinder without fins, can be seen in Fig. 6a. In this figure, the frequency around 0.174 which has the maximum power density is identified as the main frequency of the vortex shedding. Such a behavior (having one distinct frequency) can be seen in the flow over other kinds of bluff bodies with smooth surface. But, in flows over bodies with sharp edges, because of the sub-separations of flow near sharp trailing edges, some minor frequencies appear. Therefore, in Fig. 6b for the cylinder with 4 fins, in addition to the main vortex shedding frequency (around 0.143), which is produced by the bulk flow within the von-Karman vortex street, there is a secondary frequency near 0.41 that is related to the vortices induced by the edges of 2 new fins. A similar trend is seen for Fig. 6c corresponding to the case with 6 fins. The frequencies of the edge-induced vortices, which were illustrated in Fig. 5 are identified in Fig. 6c by circles. It is obvious that in this case three weak frequencies of 0.04, 0.2, and 0.37 become visible in the spectrum.

Fig. 6d represents the FFT spectrum of the lift coefficient for flow over a cylinder with 8 fins at the Reynolds number of 150. In this figure in addition to the main Karman frequency specified by a circle on the figure (about 0.145), there are two minor tips with the frequencies of 0.07 and 0.22 denoted by the ellipse and square symbols, respectively. The frequency of 0.22 is related to

the vortices induced by fins number 6 and 7, and the frequency related to the third weak summit is produced by fins number 4 and 5, which have less influence on the main flow structure. Fig. 6e shows the FFT diagram of the lift coefficient of the cylinder with 10 fins. In this figure, one more peak appears relative to case c with 8 fins. This new peak is produced by vortices shedded from fins number 2 and 3.

It should be noted that the existence of more than one major frequency is important because, if the forced oscillation frequency or the natural frequency of the structure overlap with one of these secondary frequencies the semi-lock-on phenomena will happen. The lock-on condition is similar to the resonance phenomenon in the vibration of solid structures. Particularly, if the structure has more than one natural frequency, the resonance can occur in various frequencies and oscillation modes. Similarly, in this kind of flows which has several main vortex shedding frequencies, the lock-on can happen in more than one frequency.

A non-dimensional form of the vortex shedding frequency is known as the Strouhal number. It is necessary to recall that in the remaining part of the paper, the presented Strouhal number refers to the dominant vortex shedding frequency and other frequencies will be ignored. Also it is obvious from Fig. 6 that by adding fins, the Strouhal number decreases from 0.17 for unfinned cylinder to 0.125 by inserting fins. A similar trend is reported by

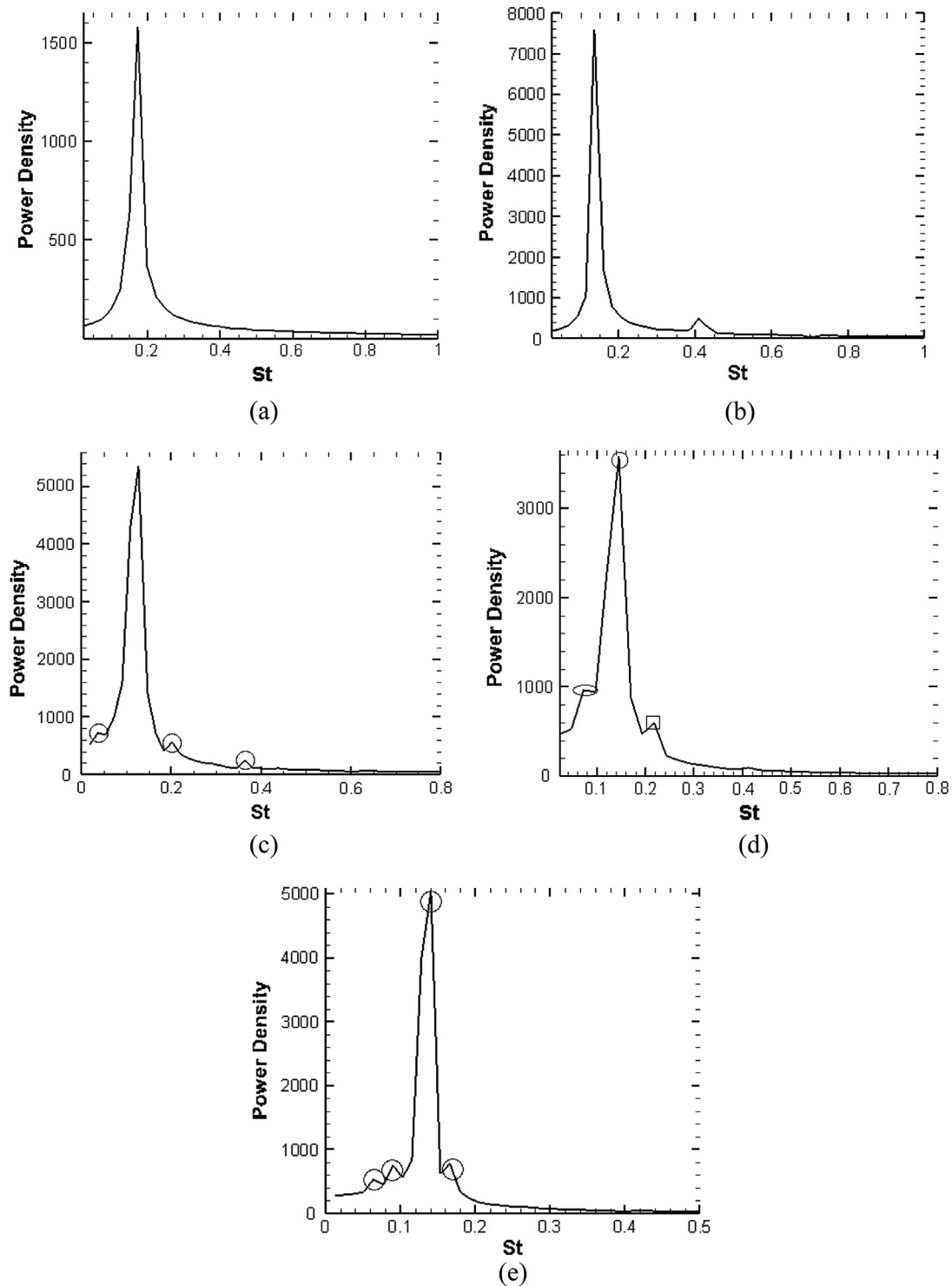


Fig. 6. Power density spectra of the lift coefficient at the Reynolds number of 150 for (a) the cylinder without fin, (b) the cylinder with 4 fins, (c) the cylinder with 6 fins, (d) the cylinder with 8 fins, (e) the cylinder with 10 fins.

Breuer et al. [46]. They found that the Strouhal number for the cylinder with square section shape is less than that of the cylinder with circular cross section. This point helps us to conclude that the existence of sharp edges in flow front reduces the Strouhal number.

The effect of fins' height on the Strouhal number is illustrated in Fig. 7. The simulations were conducted for the cylinder with 8 fins at the Reynolds number of 150. The first point in this figure belongs to the simple unfinned cylinder. It is clear that the Strouhal num-

ber for the cylinder with fins of height equal to 1.5 is approximately the half of St for unfinned case. This case is in agreement with the discussion presented after Fig. 6 about the effect of the sharp edges on the Strouhal number. It is obvious that by attaching a longer insert, the effect of the sharp trailing edge on the flow field grows and the Strouhal number experiences a more reduction.

Fig. 8 compares the variation of the Strouhal number versus the Reynolds number for two cases of cylinder with 8 and 0 fins. As it

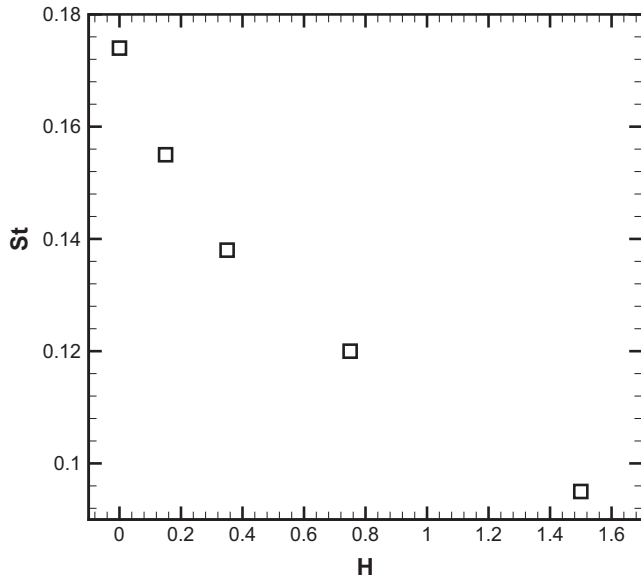


Fig. 7. Variation of Strouhal number with respect to the fin's non-dimensional height for the case of cylinder with 8 fins and Reynolds number of 150.

is expected, with the increase of the Reynolds number, the Strouhal number increases. This trend stems from the fact that the inertia force and the non-linear terms in the substantial derivative become dominant by increasing the Reynolds number. In the case of finned cylinder the Strouhal number obeys a similar trend, but with a gentler slope.

Fig. 9 demonstrates the effect of number of fins on the Strouhal number at various Reynolds numbers. It is clear that by adding fins, the Strouhal number first decreases then increases, and finally, slightly decreases. The initial descending trend was discussed in previous section. This downward tendency is related to the entrance of sharp tips into the bulk flow. By comparing the orientation of fins in the cases with 4 and 8 fins in **Fig. 1**, it is clear that fins number 6 and 7 were totally buried in the wakes of fins number 4 and 5. So, the Strouhal number is not affected by adding two extra fins number 6 and 7. Consequently, the values of St with 4

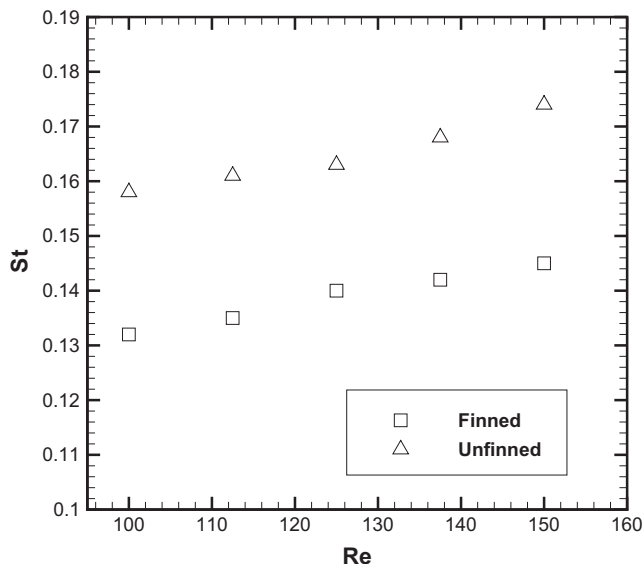


Fig. 8. Variation of Strouhal number with respect to the Reynolds number in two cases without fins and with 8 fins and non-dimensional height of 0.35.

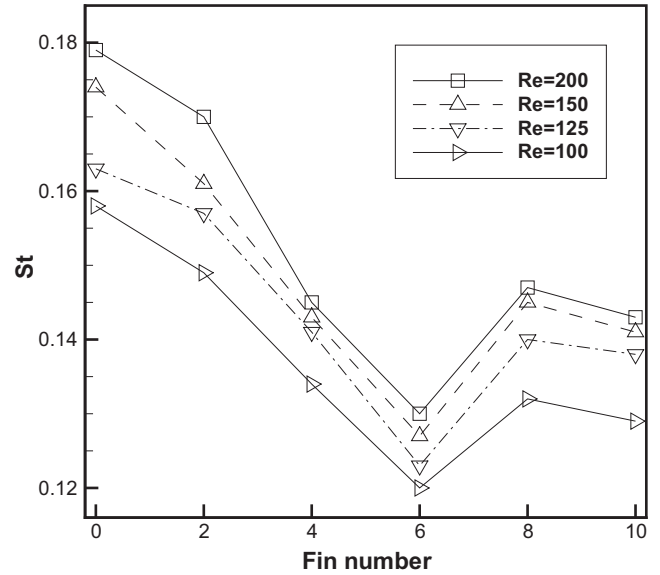


Fig. 9. Variation of the Strouhal number with respect to the fin number at four different Reynolds numbers with the non-dimensional height of 0.35.

and 8 fins are approximately the same. The final slight reduction in the Strouhal number again originates from changing the orientation of fins by adding two extra fins. With 10 fins, once more new sharp edges enter the flow field and a little decrease in St is captured.

Due to some cost reduction maneuvers and lifetime enhancement, the thermal design of extended surfaces without considering corresponding flow characteristics is not logical. So in this part, the drag coefficient for flow over the cylinder with various arrangements of fins is computed, and its dependency on the fin's height and the number of inserts is presented.

Fig. 10 shows the variation of C_d with respect to the number of fins at $Re = 100, 125, 150, 200$. The interesting point in this figure is about the case with 2 fins, which are attached to the front and rear stagnation points. **Fig. 10** indicates that by adding two horizontal fins, the drag coefficient slightly decreases. In this case the attached fins act like two attached upstream and downstream splitters, which suppress the drag force [13]. This reduction comes from the formation of a low pressure zone near the stagnation point of the cylinder due to the boundary layer separation over the upstream fin (#1). Also, the downstream fin increases the base pressure by suppressing the vortex shedding, which again leads to the reduction of C_d .

The data in **Fig. 10** for finned cases indicate that the drag coefficient suddenly experiences about 70% increase relative to the unfinned case. Then, by increasing the number of fins, the drag coefficient gradually starts to decrease. For the case with 4 fins, 2 new vertical plates are added right in front of flow. This geometry will lead to the creation of a thick wake due to the separation of flow from the tips of two vertical fins, and the augmentation of the form drag. As a result, approximately 70% enhancement of the profile drag is obtained.

But, for cases with 6, 8, and 10 fins, the effect of secondary flows inside the cavities created between two adjacent fins on the bulk flow decreases, and the whole geometry acts like a single cylinder with a larger diameter. Hence, the effect of sharp edges of fins on the flow separation is repressed, and the Karman street is suppressed. So, the drag coefficient starts to decrease. For the sake of clarity, **Fig. 11** represents the trace of two sample streamlines for two cases with 6 and 10 fins. This figure shows that the flow more effectively hugs the cylinder with more inserted fins, and the

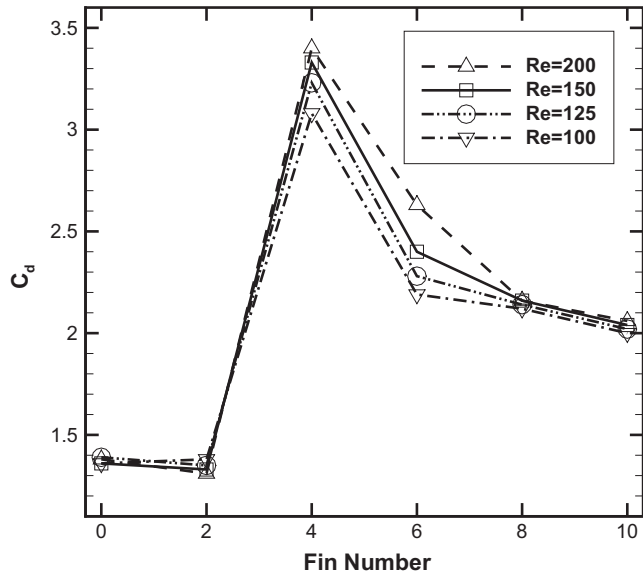


Fig. 10. The variation of the drag coefficient with respect to the number of fins attached to the cylinder with the non-dimensional height of 0.35 at different Reynolds numbers.

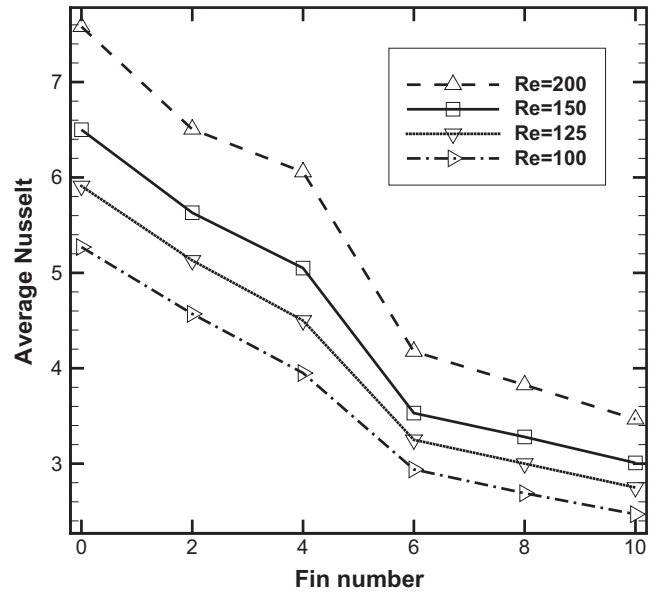


Fig. 13. The variation of averaged Nusselt number with respect to the number of fins attached to cylinder with non-dimensional height of 0.35 at different Reynolds numbers.

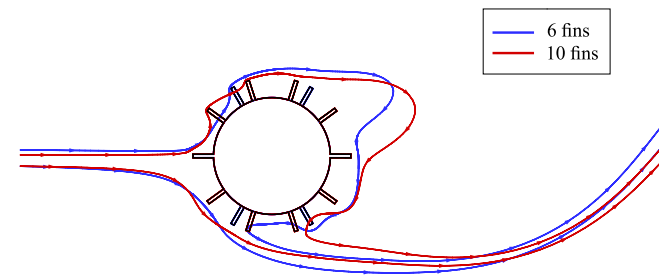


Fig. 11. Comparison of two sample streamlines for (a) the cylinder with 6 fins, the blue lines; (b) the cylinder with 10 fins, the red lines. (For interpretation of the references to color in this figure legend, the reader is referred to the web version of this article.)

streamlines remain closer to the fin tips. Inversely, a stronger vortical flow created within a bigger inter-fin cavity causes the formation of a wider downstream wake and larger drag force.

The variation of drag coefficient with respect to the fin’s normalized height for the case with 8 fins at the Reynolds number of 150 is presented in Fig. 12. It is obvious from figure that by the increase of non-dimensional height of fins, the effects of sharp edges more penetrates into the flow bulk and the separated flow region is widened. So, the low-pressure zone created behind the cylinder grows and the form drag increases. As it can be seen in Fig. 12, by lengthening the fins up to the non-dimensional height of 1.5, the drag coefficient experiences nearly 160% growth.

Fig. 13 illustrates the average Nusselt number variation with respect to the number of fins with the height of 0.35 at different Re in the range 100–200. Fig. 13 indicates that by the increase of the fin number, the Nusselt number decreases. This reduction

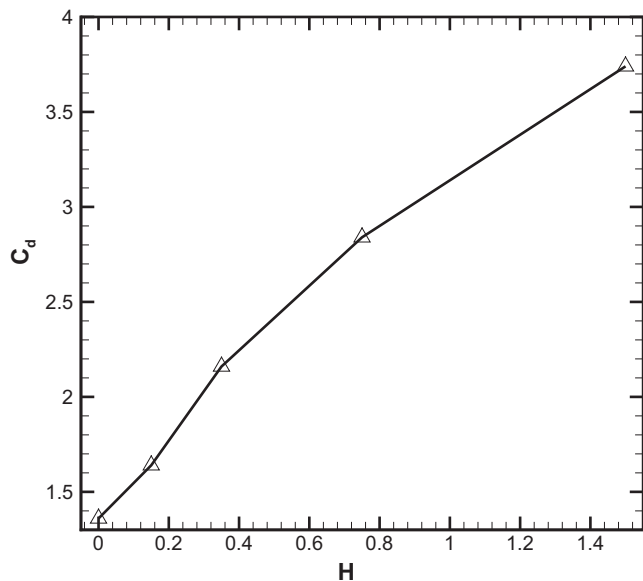


Fig. 12. Variation of drag coefficient with respect to the non-dimensional height of fins attached to the cylinder at the Reynolds number of 150.

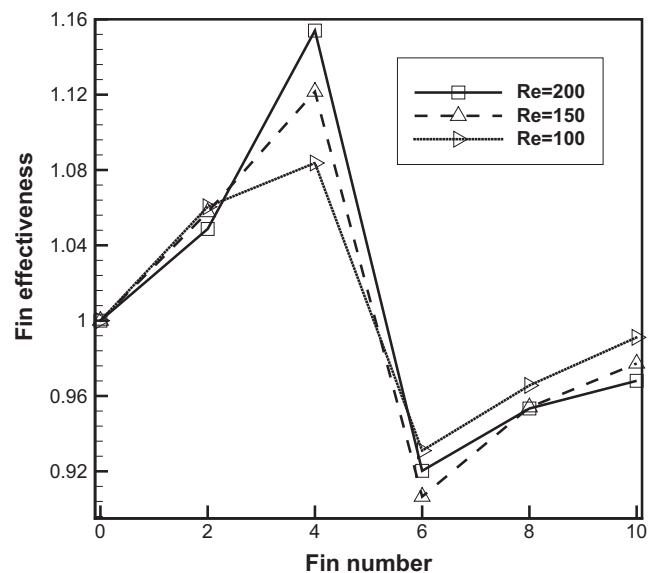


Fig. 14. The fin effectiveness with respect to the number of fins attached to the cylinder with the height of 0.35 at different Reynolds numbers.

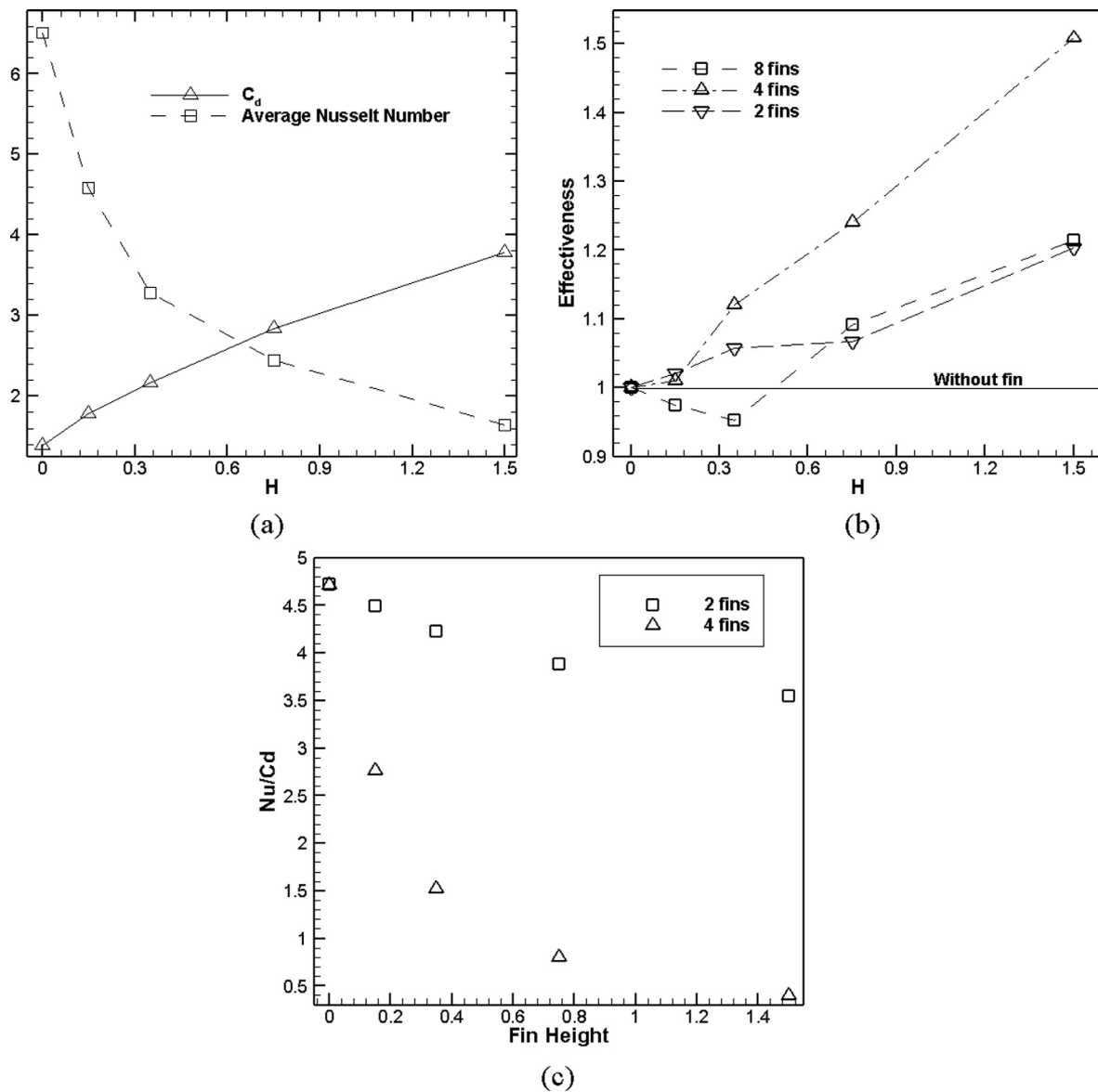


Fig. 15. The effect of fin height on (a) the drag coefficient and the Nusselt number with 8 inserts, (b) the fin effectiveness for the cylinder with 2, 4, and 8 fins, (c) Nu/C_d for finned cylinder with 2 and 4 inserts, at the Reynolds number of 150.

originates from the creation of cavities between two adjacent inserts, which weakens the convective strength of the near-body flow. It means that the low-velocity fluid enters the traps between fins, and the bulk flow with high inertia is just in contact with thin fin tips. By comparing the data in Figs. 10 and 13 it can be concluded that without regarding the extension of heat transfer over all surface for cases with higher number of fins, the best Nu/C_d ratio can be obtained for the cylinder with 2 parallel-flow horizontal fins.

In order to evaluate the efficacy of extended surfaces, the effectiveness of fins is defined as the ratio of heat transfer from the fin to the heat transfer if the fin is neglected. The effectiveness can be formulated as the division of average Nusselt number for cylinder with fin cross its related area to the Nu of naked cylinder cross naked area. This parameter measures the performance of heat transfer augmentation due to the fin attachment. Variation of the fin effectiveness at different Reynolds numbers for cylinders with fins of 0.35 height and various number of fins is illustrated in Fig. 14. This figure shows that the optimum number of fins for

which the maximum heat transfer enhancement can be obtained is 4. Also, it is obvious that the maximum effectiveness increases by increasing the Reynolds number.

With the purpose of illustrating the effect of height of inserts on thermal performance of the cylinder, Fig. 15a illustrates the variation of C_d and Nu with respect to the length of fins. This figure shows that by increasing the length of fins, due to the formation of a wider low-pressure wake, the drag coefficient remarkably increases. It is obtained that the drag coefficient for the fin length of 1.5 is approximately 9 times greater than C_d for the naked cylinder. In a reverse manner, the Nusselt number experiences a notable reduction by lengthening the inserts ($Nu_{H=1.5} = \frac{1}{10} Nu_{NoFin}$). This trend originates from the creation of dead regions between fins, which leads to a weak heat transfer rate.

Fig. 15b demonstrates the influence of fin length on the effectiveness of the fin network for three arrangements corresponding to 2, 4, and 8 fins. This figure shows that the increasing the fin length has greatest favorable effect for the case with 2 and 4 fins. But, for the cylinder with 8 inserts up to the dimensionless height

of 0.35, lengthening fins greatly reduces the Nusselt number, so that the area extension cannot compensate it. So, the fin effectiveness slightly decreases. But, for the lengths higher than 0.35 this trend is reversed. Again, it can be concluded that the height of fins has the most complimentary effect on thermal performance of fins for the cylinder outfitted with 2 and 4 inserts.

If we want to interpret this trend from the mathematical viewpoint, we can say from Fig. 15a that the slope of reduction of the Nusselt number decreases by lengthening the fins. On the other hand, by increasing the length of fins the heat transfer area linearly increases. So, it is expected that the effectiveness, which is equal to the ratio of the product of area and Nu for finned and unfinned cases, behaves like a linear function as H grows. It is interesting that a similar linear trend at high H is also captured for other fin numbers.

The fin effectiveness unlike the fin efficiency has no final limit. However, a limiting case can be constructed regarding the drag coefficient. It means that the decrease of Nu takes place as the C_d increases, and Nu/C_d has an asymptotically behavior. Fig. 15c illustrates the variation of Nu/C_d versus H . It is seen from this figure that by lengthening the fins, this ratio asymptotically decreases. Also, as obtained previously, 2-fins configuration has a larger Nu/C_d ratio in comparison with the 4-fin cylinder.

6. Conclusions

The study of flow and temperature fields for the cylinder with a variety of orientations of the radial fins and various numbers and heights was presented. The drag coefficient, the Nusselt number, and the Strouhal number were validated by existing numerical and experimental results. The spectral analysis of flow field, the fins effect on the generation of secondary frequencies, and the influence of fin's height and number of fins on the Strouhal number and drag coefficient have been investigated. It was obtained that by the increase of fin's height, the Strouhal number decreases, and the drag coefficient grows. It's concluded that with attaching 2 fins, the fins act like splitter plates which suppresses the drag coefficient. But, by adding extra fins, this trend is reversed. So, without regarding the extension of heat transfer surface for cases with higher number of fins, the best Nu/C_d ratio was obtained for the cylinder with 2 parallel-flow horizontal inserts. After computing the average Nu , the fin effectiveness has been calculated. This analysis showed that the case of cylinder with 4 fins gives the best performance.

References

- [1] A. Roshko, On the Drag and Shedding Frequency of Two-dimensional Bluff Bodies, *NacaTN*, 3169.
- [2] J.H. Gerrard, The mechanics of the formation region of the vortices behind bluff bodies, *J. Fluid Mech.* 25 (1966) 401–413.
- [3] E.R.G. Eckert, Distribution of heat transfer coefficients around circular cylinder in cross flow at Reynolds numbers from 20 to 500, *Trans. ASME* 74 (1952) 343–347.
- [4] C. Csernyei, A.G. Straatman, Forced convective heat transfer on a horizontal circular cylinder due to multiple impinging circular jets, *Appl. Therm. Eng.* 105 (2016) 290–303.
- [5] H.R. Seyf, M.R. Wilson, Y. Zhang, H.B. Ma, Flow and heat transfer of nanoencapsulated phase change material slurry past a unconfined square cylinder, *J. Heat Transfer* 136 (5) (2014) 051902.
- [6] C.H.K. Williamson, Vortex dynamics in the cylinder wake, *Annu. Rev. Fluid Mech.* 28 (1996) 477–539.
- [7] G.H. Koopman, The vortex wakes of the vibrating cylinders at low Reynolds numbers, *J. Fluid Mech.* 28 (1967) 1007–1015.
- [8] M.R.H. Nobari, J. Ghazanfarian, A numerical investigation of fluid flow over a rotating cylinder with cross flow oscillation, *Comput. Fluids* 38 (2009) 2026–2036.
- [9] J. Ghazanfarian, M.R.H. Nobari, A numerical study of convective heat transfer from a rotating cylinder with cross-flow oscillation, *Int. J. Heat Mass Transfer* 52 (2009) 5402–5411.
- [10] Gustavo R.S. Assi, Peter W. Bearman, Transverse galloping of circular cylinders fitted with solid and slotted splitter plates, *J. Fluids Struct.* 54 (2015) 263–280.
- [11] Y. Qiu, Y. Sun, Y. Wu, Y. Tamura, Effects of splitter plates and Reynolds number on the aerodynamic loads acting on a circular cylinder, *J. Wind Eng. Ind. Aerodynam.* 127 (2014) 40–50.
- [12] J.Y. Hwang, K.S. Yang, Drag reduction on a circular cylinder using dual detached splitter plates, *J. Wind Eng. Ind. Aerodynam.* 95 (2007) 551–564.
- [13] C. Bayram, U. Akdag, S. Gunes, A. Beskok, Flow past an oscillating circular cylinder in a channel with an upstream splitter plate, *Phys. Fluids* 10 (2008) 27–42.
- [14] S.C. Haldar, G.S. Kochhar, K. Manohar, R.K. Sahoo, Numerical study of laminar free convection about a horizontal cylinder with longitudinal fins of finite thickness, *Int. J. Therm. Sci.* 46 (2007) 692–698.
- [15] R. Sajedi, M. Jafari, M. Taghilou, Experimental and numerical study on the optimal fin numbering in an external extended finned tube heat exchanger, *Appl. Therm. Eng.* 83 (2015) 139–146.
- [16] A.K. Abuhijleh, Numerical simulation of forced convection heat transfer from a cylinder with high conductivity radial fins in cross-flow, *Int. J. Therm. Sci.* 42 (2003) 741–748.
- [17] H.R. Seyf, M. Feizbakhshi, Computational analysis of nanofluid effects on convective heat transfer enhancement of micro-pin-fin heat sinks, *Int. J. Therm. Sci.* 58 (2012) 168–179.
- [18] H.R. Seyf, M. Layeghi, Numerical analysis of convective heat transfer from an elliptic pin fin heat sink with and without metal foam insert, *J. Heat Transfer* 132 (7) (2010) 071401.
- [19] B. Rajabifar, H.R. Seyf, Y. Zhang, S.K. Khanna, Flow and heat transfer in micro pin fin heat sinks with nano-encapsulated phase change materials, *J. Heat Transfer* 138 (6) (2016) 062401.
- [20] E. Tian, Y.L. He, W.Q. Tao, Numerical simulation of finned tube bank across a staggered circular-pin-finned tube bundle, *Numer. Heat Transfer A* 68 (7) (2015) 737–760.
- [21] Y. Jin, Z.Q. Yu, G.H. Tang, Y.L. He, W.Q. Tao, Parametric study and multiple correlations of an H-type finned tube bank in a fully developed region, *Numer. Heat Transfer A* 70 (1) (2016) 64–78.
- [22] E. Martinez-Espinosa, W. Vicente, M. Salinas-Vazquez, I. Carvajal-Mariscal, Numerical analysis of turbulent flow in a small helically segmented finned tube bank, *Heat Transfer Eng.* 38 (1) (2017) 47–62.
- [23] A. Tripathi, A.K. Singh, A review on heat transfer and pressure drop correlations in solid circular finned tube bundles positioned at inline and staggered arrangement in cross flow, *Int. J. Res. Aeronaut. Mech. Eng.* 3 (3) (2015) 61–67.
- [24] H.R. Seyf, A. Henry, Thermophotovoltaics: a potential pathway to high efficiency concentrated solar power, *Energy Environ. Sci.* 9 (8) (2016) 2654–2665.
- [25] Z. Liu, Y. Liu, Y. Chang, H.R. Seyf, A. Henery, A.L. Mattheyses, K. Yehl, Y. Zhang, Z. Huang, K. Salaita, Nanoscale optomechanical actuators for controlling mechanotransduction in living cells, *Nat. Methods* 13 (2016) 143–146.
- [26] A. Shalchi-Tabrizi, H.R. Seyf, Analysis of entropy generation and convective heat transfer of Al_2O_3 nanofluid flow in a tangential micro heat sink, *Int. J. Heat. Mass Transfer* 55 (2012) 4366–4375.
- [27] H.R. Seyf, Z. Zhou, H.B. Ma, Y. Zhang, Three dimensional numerical study of heat-transfer enhancement by nano-encapsulated phase change material slurry in microtube heat sinks with tangential impingement, *Int. J. Heat Mass Transfer* 56 (1) (2013) 561–573.
- [28] A. Malli, H.R. Seyf, M. Layeghi, S. Sharifan, H. Behraves, Investigating the performance of cellulosic evaporative cooling pads, *Energy Convers. Manage.* 52 (7) (2011) 2598–2603.
- [29] M. Layeghi, M. Karimi, H.R. Seyf, A numerical analysis of thermal conductivity, thermal dispersion, and structural effects in the injection part of the resin transfer molding process, *J. Porous Media* 13 (4) (2010) 375–385.
- [30] H.R. Seyf, M. Layeghi, Vapor flow analysis in flat plate heat pipes using homotopy perturbation method, *J. Heat Transfer* 132 (5) (2010) 054502.
- [31] H.R. Seyf, S. Kim, Y. Zhang, Thermal performance of an Al_2O_3 water nanofluid pulsating heat pipe, *J. Electron. Packaging* 135 (2013) 0310041–0310049.
- [32] J. Jiin-Yuh, Y. Jyh-Yau, Experimental and 3-D numerical analysis of the thermal-hydraulic characteristics of elliptic finned tube heat exchangers, *Heat Transfer Eng.* 19 (4) (1998) 55–67.
- [33] A. Lemouedda, A. Schmid, E. Franz, M. Breuer, A. Delgado, Numerical investigations for the optimization of serrated finned-tube heat exchangers, *Appl. Therm. Eng.* 31 (8) (2011) 1393–1401.
- [34] J.-Y. Hwang, K.S. Yang, Drag reduction on a circular cylinder using dual detached splitter plates, *J. Wind Eng. Ind. Aerodynam.* 95 (7) (2007) 551–564.
- [35] B.G. Dehkordi, H.H. Jafari, On the suppression of vortex shedding from circular cylinders using detached short splitter-plates, *J. Fluids Eng.* 132 (4) (2010) 044501.
- [36] G.E. Karniadakis, G.S. Triantafyllou, Three-dimensional dynamics and transition to turbulence in the wake of bluff objects, *J. Fluid Mech.* 238 (1992) 130.
- [37] J. Ghazanfarian, D. Ghanbari, Computational fluid dynamics investigation of turbulent flow inside a rotary double external gear pump, *J. Fluids Eng.* 137 (2) (2015) 021101.
- [38] J. Robichaux, S. Balachandar, S.P. Vanka, Three-dimensional Floquet instability of the wake of square cylinder, *Phys. Fluids* 11 (1999) 560.
- [39] Openfoam User's Guide, Version 2.3, 2014, <<http://www.OpenFOAM.com>>.
- [40] N.M. Sudharsan, V.A. Jambekhar, V. Babu, A validation study of OpenFOAM using the supersonic flow in a mixed compression intake, *Proc. Inst. Mech. Eng. Part G: J. Aerospace Eng.* 224 (6) (2010) 673–679.

- [41] Koji Miyaji, Kozo Fujii, Numerical analysis of three-dimensional shock/shock interactions and the aerodynamic heating, in: American Institute of Aeronautics and Astronautics, AIAA, 1999, pp. 1–10.
- [42] J. Martinez, Large Eddy Simulation Analysis of Non-reacting Sprays Inside a High-g Combustor, 2012.
- [43] M. Gramlich, Numerical Investigations of the Unsteady Flow in the Stuttgart Swirl Generator with OpenFOAM, 2012.
- [44] T. Besenic, Implementation and Validation of the Two-Potential Electrolyte Assembly Equations in the Computational Fuel Cell Model, 2016.
- [45] T. Tamura, On the reliability of two-dimensional simulation for unsteady flows around a cylinder-type structure, *J. Wind Eng. Ind. Aerodynam.* 35 (1990) 275–298.
- [46] M. Breuer, J. Bernsdorf, T. Zeiser, F. Durst, Accurate computations of the laminar flow past a square cylinder based on two different methods: lattice-Boltzmann and finite-volume, *Int. J. Heat Fluid Flow* 21 (1999) 186–196.
- [47] R. Henderson, Nonlinear dynamics and pattern formation in turbulent wake transition, *Int. J. Fluid Mech.* 352 (1997) 65–112.
- [48] J. Park, K. Kwon, H. Choi, Numerical solutions of flow past a circular cylinder at Reynolds numbers up to 160, *KSME Int. J.* 12 (1998) 1200–1205.
- [49] R. Hilpert, Wärmeabgabe von geheizten Drhten und Rohren im Luftstrom, *Forsch. Geb. Ingenieurwes* 4 (1933) 215.
- [50] S.W. Churchill, M. Bernstein, A correlating equation for forced convection from gases and liquids to a circular cylinder in crossflow, *J. Heat Transfer* 99 (1977) 300–306.